2011

Determining individual mineral contributions to U(VI) adsorption in a contaminated aquifer sediment: A fluorescence spectroscopy study

Zheming Wang
Pacific Northwest National Laboratory, Zheming.wang@pnl.gov

John M. Zachara
Pacific Northwest National Laboratory, john.zachara@pnl.gov

Jean-Francois Boily
Umea University, jean-francois.boily@chem.umu.se

Yuanxian Xia
Pacific Northwest National Laboratory

Tom C. Resch
Pacific Northwest National Laboratory

See next page for additional authors

Available online at www.sciencedirect.com
ScienceDirect
Geochimica et Cosmochimica Acta 75 (2011) 2965–2979
Geochimica et Cosmochimica Acta
www.elsevier.com/locate/gca

Determining individual mineral contributions to U(VI) adsorption in a contaminated aquifer sediment: A fluorescence spectroscopy study

Zheming Wang *, John M. Zachara, Jean-François Boily [1], Yuanxian Xia, Tom C. Resch, Dean A. Moore, C. Liu

Pacific Northwest National Laboratory, Richland, WA 99352, USA

Received 1 November 2010; accepted in revised form 23 February 2011; available online 10 March 2011

Abstract

The adsorption and speciation of U(VI) was investigated on contaminated, fine grained sediment materials from the Hanford 300 area (SPP1 GWF) in simulated groundwater using cryogenic laser-induced U(VI) fluorescence spectroscopy combined with chemometric analysis. A series of reference minerals (montmorillonite, illite, Michigan chlorite, North Carolina chlorite, California clinochlore, quartz and synthetic 6-line ferrihydrite) was used for comparison that represents the mineralogical constituents of SPP1 GWF. Surface area-normalized K_d values were measured at U(VI) concentrations of 5×10^{-7} and 5×10^{-6} mol L^{-1} that displayed the following affinity series: 6-line-ferrihydrite > North Carolina chlorite ≈ California clinochlore > quartz ≈ Michigan chlorite > illite > montmorillonite. Both time-resolved spectra and asynchronous two-dimensional (2D) correlation analysis of SPP1 GWF at different delay times indicated that two major adsorbed U(VI) species were present in the sediment that resembled U(VI) adsorbed on quartz and phyllosilicates. Simulations of the normalized fluorescence spectra confirmed that the speciation of SPP1 GWF was best represented by a linear combination of U(VI) adsorbed on quartz (90%) and phyllosilicates (10%). However, the fluorescence quantum yield for U(VI) adsorbed on phyllosilicates was lower than quartz and, consequently, its fractional contribution to speciation may be underestimated. Spectral comparison with literature data suggested that U(VI) exist primarily as inner-sphere complexes with surface silanol groups on quartz and as surface U(VI) tricarbonate complexes on phyllosilicates.
Published by Elsevier Ltd.

1. INTRODUCTION

Uranium is a major radioactive contaminant at former US Department of Energy nuclear weapons sites (DOE, 1995, 2001) and numerous locations worldwide (Bernhard et al., 1998; Geipel et al., 2007). Uranium primarily exists in the +6 oxidation state as the divalent uranyl ion (UO_2^{2+}) under aerobic conditions. For the large majority of contaminated soil and sediment sites where the overall uranium concentration is low (<25 mg kg^{-1}), the concentration of dissolved uranium in the aqueous phase is determined by its surface complexation to various mineral phases (Chisholm-Brause et al., 2004; Catalano and Brown, 2005; Arai et al., 2006; Zachara et al., 2007; Bond et al., 2008).

Iron oxides, calcium carbonate, quartz/amorphous silica and phyllosilicates can all be important U(VI) adsorbents in subsurface materials (Morris et al., 1994; Reeder et al., 2000; Gabriel et al., 2001; Reeder et al., 2001; Duff et al., 2002; Chisholm-Brause et al., 2004; Kohler et al., 2004; Chang et al., 2006; Fox et al., 2006). Subsurface sediments are heterogeneous mixture of mineral phases. Multiple adsorbent phases may be present that simultaneously

* Corresponding author. Address: Pacific Northwest National Laboratory, P.O. Box 999, MS K8-96, Richland, WA 99354, USA. Tel.: +1 509 371 6349; fax: +1 509 371 6354.
E-mail addresses: Zheming.Wang@pnl.gov (Z. Wang), jean-francois.boily@chem.umu.se (J.-F. Boily).
[1] Present address: Umea University, Sweden.

0016-7037/$ - see front matter Published by Elsevier Ltd.
doi:10.1016/j.gca.2011.03.008

interact with, and control aqueous U(VI) concentrations by surface complexation. Knowledge of the surface complexed species and the host mineral phases (surface speciation) can support a robust understanding of the adsorption process for geochemical modeling. Surface speciation is a complex state defined by properties of the reactive mineral phases (surface area, site concentration, intrinsic affinity) and aqueous composition (pH, ligands, etc.). It is also temporarily variable as it may change in response to changes in groundwater composition. Thus, for any particular subsurface contaminant plume, the relative importance of specific mineral phases depends on a number of different factors, and can be difficult to predict.

The scientific ability to accurately describe uranium speciation in soils and subsurface sediments is not comprehensive. For sediments, aside from incomplete identification of the mineralogic components and their key properties, low solid (<25 mg kg^{-1}) and aqueous U(VI) concentrations ($<10^{-6}$ mol L^{-1}) are common (Bond et al., 2008; Um et al., 2010). Many spectroscopic techniques that are capable of revealing U speciation in mineral materials, such as extended X-ray absorption fine structure (EXAFS) (Hudson et al., 1999; Elzinga et al., 2004), Fourier-transfer infrared spectroscopy (FTIR) (Bargar et al., 1999), and Raman spectroscopy (Morris et al., 1994), suffer from low sensitivity and are unable to produce data with satisfactory quality at commonly observed environmental concentrations. Time-resolved laser-induced fluorescence (TRLIF) spectroscopy, particularly when performed at cryogenic temperatures, is one technique that offers high sensitivity and spectral resolution for the identification of U(VI) speciation in complex natural sediments, sediment porewaters, and other media at low U(VI) concentrations (Morris et al., 1996; Hunter and Bertsch, 1998; Duff et al., 2000; Wang et al., 2004a,b, 2005; Chang et al., 2006; Grossmann et al., 2009; Wan et al., 2009).

Here we applied a combination of laboratory adsorption measurements and liquid helium temperature (LHeT) TRLIF spectroscopy to investigate the speciation of adsorbed U(VI) at low concentration on an aquifer sediment. A series of seven reference phases that were representative of potential adsorbents in the sediment (chlorites, smectite, illite, ferrihydrite and quartz) were studied in parallel. The fluorescence spectra of U(VI) on the naturally contaminated and a lab-spiked subsample were similar, and displayed contributions from multiple surface species. These spectra were successfully reconstructed from those of a subset of the reference phases (quartz and phyllosilicates) using chemometric methods.

2. MATERIALS AND EXPERIMENTAL DETAILS

2.1. U(VI)-bearing aquifer sediment

A silt-textured size fraction of air-dried contaminated aquifer sediment (SPP1 GWF) was obtained by centrifugation and filtration of the ground water collected at 20 feet below ground level in the vadose zone of a historic waste disposal pond in Hanford 300 area (Zachara et al., 2005). No further treatment was applied to these sediments. Selected properties of this material which contains 0.13 mmol kg^{-1} contaminant U are listed in Tables 1 and 2.

Table 1
A Summary of SPP1 GWF mineralogical characteristics.

Size distribution	Sand (15.7%), Silts (73.6%), Clay (10.7)
Mineralogy	Quartz, feldspars, phyllosilicates[a]
Clay mineralogy	Smectite (40%), illite (45%), chlorite (15%), quartz (4%)
Surface area of bulk sediment[b]	62.8 m^2 g^{-1}
Surface area of clay fraction[b]	91.8 m^2 g^{-1}

[a] SPP1 GWF also contains 1.3% crystalline Fe oxides and 0.5% poorly crystalline Fe oxide (Bond et al., 2008).
[b] N_2 BET surface area.

Table 2
Reference phase mineral properties.

Mineral	Size (μm)	Total Fe (wt.%)	Surface area (m^2 g^{-1})	Source
Montmorillonite (SWy-1)[a]	⩽2	3.1	31.0	[(Zachara et al., 1993)]
Fithian illite[a]	⩽2	4.6	87.0	This work
Michigan chlorite C[a]	2–5	27.9	15.2	This work
Michigan chlorite S	5–20	27.9	4.42	This work
N.C. chlorite C[a]	2–5	0.74	26.5	This work
N.C. chlorite S	5–20	0.74	14.1	This work
Calif. clinochlore C[a]	2–5	1.1	17.3	This work
Calif. clinochlore S	5–20	1.1	5.57	This work
Quartz	8–30	0	0.33	This work
6-Line Fh	~2	62.9	200–300	[(Schwertmann and Cornell, 2000)]
SPP1 GW fines	0.1–20	6.2	62.9	This work

[a] The molecular formulae are: Montmorillonite: $(Ca_{0.001}K_{0.003}Na)[Al_{3.04}Fe(III)_{0.41}Mg_{0.532}](Si_{7.85}Al_{0.147})(OH)_4O_{20}$ (Zachara et al., 1993); Fithian illite: $K_{0.86}Na_{0.11}Ca_{0.07}(Si_{6.95}Al_{1.05})[Al_{2.87}Fe_{0.67}Mg_{0.47}]O_{20}(OH)_4$ (Seabaugh et al., 2006); Michigan chlorite: $(Mg_{0.56}Al_{0.60}Fe2+_{1.78})(Si_{2.47}Al_{1.53})O_{10}(OH)_2.(Mg_{0.49}Al_{1.00}Fe^{2+}{}_{1.51})(OH)_6$ (Nelson and Guggenheim, 1993); N.C. Chlorite: $g_{2.97}Al_{0.03})(Si_{3.02}Al_{0.98})O_{11}(OH)_2.(Mg_{1.98}Al_{0.69}Cr_{0.23}Fe^{3+}{}_{0.04}Fe^{2+}{}_{0.04}Ni_{0.02})(OH)_6$ (Phillips et al., 1980; Nelson and Guggenheim, 1993); California clinochlore: $Mg_{2.95}Al_{0.05})(Si_{2.99}Al_{1.01})O_{10}(OH)_2.(Mg_{1.97}Al_{0.66}Cr_{0.25}Fe^{3+}{}_{0.06}Fe^{2+}{}_{0.06})(OH)_6$ (Phillips et al., 1980).

2.2. Reference phases

Montmorillonite (SWy-1), Fithian illite, Michigan chlorite, North Carolina chlorite, California clinochlore, quartz and 6L-Fh were selected as reference phases for SPP1 GWF based on previous mineralogic analysis of sediments from this site. 6L-Fh was included because a small amount of poorly crystalline Fe(III) oxide exists in the sediment (Qafoku et al., 2005; Um et al., 2008, 2010). Ferrihydrite displays high affinity for U(VI) over broad pH range (Hsi and Langmuir, 1985; Waite et al., 1994) and has been implicated as a U adsorbent in Hanford sediments (Barnett et al., 2002).

The clay-sized fraction of SWy-1 (Source Clay Repository) was isolated and processed to remove carbonates, organics, and iron oxides (Sposito and Levesque, 1985; Kunze and Dixon, 1986; McKinley et al., 1995). Quartz (Min-U-Sil 30, Pennsylvania Glass & Sand Company) was treated to remove surface contaminants and to obtain a specific particle diameter range from 8 to 30 μm (Kohler et al., 1996). 6L-Fh was synthesized according to Schwertmann and Cornell (Schwertmann and Cornell, 2000). Fithian illite, Michigan chlorite, North Carolina chlorite, and California clinochlore were obtained from Ward's Natural Science, and were ground and sieved to obtain different size fractions (2–5 and 5–20 μm fractions). X-ray diffraction (XRD), scanning electron microscopy (SEM), and energy-dispersive X-ray spectroscopy (EDS) were performed to assess the structure, appearance, and composition of the reference phases. All adsorbents were analyzed by XRD both before and after contact with U(VI)-containing electrolytes. Selected properties of the reference phases are summarized in Table 2.

2.3. Aqueous solutions

A calcite-saturated synthetic groundwater (SGW2, pH 8.1) was prepared according to Bond et al. (2008). Uranium nitrate (1.06×10^{-3} mol L^{-1}, pH 1) was prepared as a primary stock solution. SGW2 was bubbled with air for 1 week at pH 8.1 to ensure equilibrium with atmospheric CO_2. All chemicals used were reagent grade.

2.4. Mineralogic characterization

XRD analysis of the sediment and reference mineral phases was performed on a Scintag XRD unit with a Peltier thermoelectrically cooled detector and a copper X-ray tube. XRD analysis of the mineral slurries after contact with U(VI) was performed using a Micro XRD spectrometer (Rigaku). Scans were obtained from 2° to 65° 2θ (0.01° step) with a dwell time of 2 s. The JADE® and PDF™ [Joint Committee on Powder Diffraction Standards (JCPDS), International Center for Diffraction Data (ICDD) (Newtown Square, Pennsylvania)] were used for mineralogical identification and quantification.

The clay fraction of SPP1 GWF was obtained by sedimentation after dispersion (0.001 M sodium hexametaphosphate). The clay was mounted on an aluminum slide (Drever, 1973) that was analyzed using a Rigaku D/MAX RAPID II microdiffractometer with a rotating Cr anode and micro focus optics operating at 35 kV and 25 mA.

SEM analysis was performed on a Zeiss 982 FE-SEM equipped with an Oxford Links ISIS 300 EDS operated at 20 KeV. The samples were affixed to double-sided carbon tape attached to an aluminum mounting stub. Photomicrographs of high-resolution secondary electron (SE) and backscattered electron (BSE) images were obtained as digital images.

BET surface area was determined by nitrogen adsorption/desorption (Quantachrome Autosorb 6-B). Particle-size measurements were made using a Mastersizer 2000 (Malvern Instruments, Inc., Southborough, MA 01772, USA) with a Hydro G sample dispersion accessory to decrease aggregation.

2.5. U(VI) fluorescence spectroscopy

The instrumentation and experimental procedures for fluorescence spectroscopic measurements at LHeT were described previously (Wang et al., 2004b, 2005). Samples in 2 mm × 4 mm × 25 mm quartz cuvettes were mounted on the sample holder of a CRYO Industries RC152 cryostat with liquid helium vaporizing beneath the sample. The sample was excited with a Spectra-Physics Nd:YAG laser pumped MOPO-730 laser at 415 nm, the spectral maximum of the first electronic absorption band, and the emitted light was collected at 85° to the excitation beam, dispersed through an Acton SpectroPro 300i double monochromator spectrograph, and detected with a thermoelectrically cooled Princeton Instruments PIMAX intensified CCD camera. The fluorescence decay curves were measured by a Hamamatsu R928 photomultiplier tube (PMT) and recorded with a Tektronics TDS754A digital oscilloscope.

2.6. U(VI) adsorption

Mineral adsorbents were twice equilibrated with SGW2 at pH 8.1 with phase separation by centrifugation. Adsorbent masses were adjusted to yield surface area concentrations ranging from 97.0 to 1740 m^2 L^{-1} (Table 3). The resulting solid was then re-suspended in 10 mL of SGW2 and spiked with the U(VI) stock solution to yield initial U(VI) concentrations of 5×10^{-6} or 5×10^{-7} mol L^{-1}. The initial U(VI) concentrations were undersaturated with respect to known U(VI) mineral phases. Suspension pH was adjusted to 8.1 with dilute NaOH and/or HNO_3 and re-adjusted, if necessary, during the contact period. The U-bearing suspension was then slowly agitated on an orbital shaker for 24 h, followed by phase separation by centrifugation at 2000 rcf for 30 min. The resulting solid paste and a supernatant aliquot were subjected to fluorescence analysis, while the remaining supernatant was acidified for U(VI) (KPA) and other solute analyses (ICP/MS).

2.7. Chemometric analyzes

The normalized fluorescence spectra were analyzed by Matlab (The Mathworks, Inc.). The spectra were grouped into a series of **F** matrices for each separate sample**,** consisting of m rows of wavelengths and n columns of measurements at different time delays and/or gate widths. The data were offset to average zero fluorescence values at wavelengths where U(VI) species do not fluoresce. Instrumental noise was removed from **F** by reconstructing this matrix with orthogonal vectors solely arising from the fluorescence of k U(VI) species using a Singular Value Decomposition (SVD) (Golub and Reinsch, 1970) of **F**:

$$\mathbf{F}_{\mathbf{net}} = \mathbf{U}_{m\times k} \cdot \mathbf{S}_{k\times k} \cdot \mathbf{V}^{\mathrm{T}}_{n\times k} \quad (1)$$

where **U** is a matrix of orthogonal vectors of unit length, **S** is a diagonal matrix of the singular values of the vectors **U** and $\mathbf{V}^{\mathrm{T}}$ is the transposed (T) matrix of the contributions of

Table 3
Experimental data for U(VI) adsorption at pH 8.1 and $I = 0.01$ mol L^{-1} at 25 °C.

Mineral	Mineral weight (g)	Total surface area (m^2)	$[U]_{total}$ (mol L^{-1})	U adsorbed (%)	U adsorption density $\times 10^2$ (μmol m^{-2})	K_d (mL g^{-1})	$K_{d,normalized}$ (mL m^{-2})
Montmorillonite	0.05	1.55	5.0×10^{-7}	51.2	0.17	210	6.8
Montmorillonite	0.05	1.55	5.0×10^{-6}	36.4	1.17	114	3.7
Fithian illite	0.20	17.4	5.0×10^{-7}	95.3	0.03	1014	11.7
Fithian illite	0.20	17.4	5.0×10^{-6}	89.8	0.26	440	5.1
Michigan chlorite C[a]	0.20	3.04	5.0×10^{-7}	88.5	0.15	383	25.2
Michigan Chlorite C[a]	0.20	3.04	5.0×10^{-6}	81.4	1.34	219	14.4
Michigan chlorite S[b]	0.22	0.97	5.0×10^{-7}	55.4	0.28	56.5	12.8
Michigan chlorite S[b]	0.22	0.97	$5.0 \times 10^{-}6$	30.6	1.57	20.1	4.54
NC chlorite C[a]	0.11	2.92	5.0×10^{-7}	99.6	0.17	21,982	830
NC chlorite C[a]	0.11	2.92	5.0×10^{-6}	99.7	1.71	27,003	1020
NC chlorite S[b]	0.21	2.96	5.0×10^{-7}	99.5	0.17	8666	615
NC chlorite S[b]	0.21	2.96	5.0×10^{-6}	99.6	1.68	11,279	800
Calif. clinochlore C[a]	0.17	2.94	5.0×10^{-7}	99.6	0.17	15,680	906
Calif. Clinochlore C[a]	0.17	2.94	5.0×10^{-6}	99.3	1.69	8193	474
Calif. clinochlore S[b]	0.18	1.00	5.0×10^{-7}	96.5	0.48	1545	277
Calif. clinochlore S[b]	0.18	1.00	5.0×10^{-6}	91.6	4.57	606	109
Quartz	2.50	1.00	5.0×10^{-7}	73.7	0.37	11.2	28.0
Quartz	2.50	1.00	5.0×10^{-6}	61.8	3.09	6.5	16.2
6-Line Fh	0.024	6.00[c]	5.0×10^{-7}	99.9	0.17	756,551	3030
6-Line Fh	0.024	6.00[c]	5.0×10^{-6}	99.9	1.67	344,050	1380
SPP1 GWF	0.15	9.44	5.0×10^{-7}	29.3 (85.7)[d]	0.02 (0.22)	27.6 (399.4)	0.44 (6.35)
SPP1 GWF	0.15	9.44	5.0×10^{-6}	37.0 (54.8)[d]	0.20 (0.41)	39.2 (80.9)	0.62 (1.29)

[a] Clay size fraction.
[b] Silt size fraction.
[c] The median surface area of 250 m^2 g^{-1} (Schwertmann and Cornell, 2000) was used in the calculation.
[d] Data in parenthesis were obtained after including the amount of U(VI) in the original sediment (31.3 mg kg^{-1}) (Bond et al., 2008).

every vector to each measurement condition (i.e time delays and/or gate width). The optimal number of k was determined with the Factor Indicator Function (Malinowski, 1977):

$$\mathrm{IND} = \mathrm{RSD}(k)/(n-k)^2 \tag{2}$$

where RSD(k) or residual standard deviation, is the misfit between the product $\mathbf{U}_{m\times k}\cdot\mathbf{S}_{k\times k}\mathbf{V}^{\mathrm{T}}_{n\times k}$, where values of k are sequentially tested for values of $k = [1,n]$. Noise-reduced $\mathbf{F}$ matrices were reconstructed by discarding all $>k$ orthogonal vectors associated to random noise.

Asynchronous 2D correlation plots were generated from the $\mathbf{F}_{net}$ matrix of each sample mineral using the equations of Noda and Ozaki (Ozaki et al., 2004) for spectra collected at unevenly-spaced time intervals:

$$\Psi(\nu_1-\nu_2) = \frac{1}{2(t_m-t_1)}\sum_{j=1}^{m}\tilde{F}_j(\nu_1)\cdot\left(\sum_{k=1}^{m}N_{jk}\cdot\tilde{F}_k(\nu_2)\right)\cdot(t_{j+1}-t_{j-1}) \tag{3}$$

where N_{jk} is the Hilbert-Noda transformation matrix (Ozaki et al., 2004). This map reveals changes in intensities at ν_1 and ν_2 at values of $|\psi(\nu_1,\nu_2)|_{max}$ that are *out-of-phase*, i.e. that varied sequentially or successively with time. It also enhances the spectral resolution and can be used to reveal peak components that cannot be readily shown in vector-based spectra.

Multivariate Curve Resolution (MCR) analyses were carried out on all $\mathbf{F}$ matrices with the program MCR-ALS (Jaumot et al., 2005) to resolve the time-dependent profiles and the pure spectral components ε_{sample} (arbitrary units of molar fluorescence coefficients) of every sample. The pure spectral component of the SPP1 GWF (ε_{SPP1}) was reconstructed with those of the samples exhibiting the highest degree of similarity. The spectra of SPP1 GWF, $\varepsilon_{SPP1,net}$, was modeled as a linear combination of spectral representations of m samples such that:

$$\varepsilon_{SPP1,net} = \sum_{m=1}^{m} f_m\cdot\varepsilon_{sample\ m,net} \tag{4}$$

Values of f_m were optimized using a non-linear least square method based on Levenberg–Marquardt iterations. All values of $\varepsilon_{sample\,m,net}$ were normalized for peak area.

2.8. Aqueous U(VI) speciation

The speciation of U(VI) in SGW2 under ambient conditions was calculated using the MINTEQA2 (Allison et al., 1998) software with the most current, critically reviewed thermodynamic stability constants for U(VI) complexes (Grenthe and Konings, 1992; Guillaumount et al., 2003).

3. RESULTS

3.1. Mineral characteristics

3.1.1. XRD results and general mineral properties

The SPP1 GWF bulk sample displayed X-ray diffraction maxima from quartz, feldspar, chlorite and illite (Fig. 1). Oriented mounts of the clay fraction (SPP1 GWF Clay in

Fig. 1) revealed smectite (*d*-spacing 16.9 Å when exposed to ethylene glycol), chlorite (*d*-spacing 14.2 Å), illite (*d*-spacing 9.97 Å) and quartz (*d*-spacings 4.25 and 3.34 Å). These results are consistent with the selected reference phases.

For chlorites, the relative intensities of the 0 0 *l* (l = 1, 2, . . ., 5) diffraction peaks provide information on the total Fe content and its relative distribution in the silicate and the brucite layers (Brown and Brindley, 1980; Moore and Reynolds, 1997). The diffraction peaks of the chlorite(s) in the SPP1 GWF had intensity ratios of 0.13:0.16:0.04:0.07:0.02 (for *l* values from 1 to 5). Based on the ratio of total intensity of the (0 0 2) and (0 0 4) peaks and the symmetry-corrected (0 0 3) peak, the total Fe content (*y*) was determined to be 2, based on a molecular formula of $(Mg,Al)_{6-y}Fe_y(Si,Al)_4O_{10}(OH)_8$ (Moore and Reynolds, 1997). The symmetry of Fe substitution (D), the number of Fe atoms in the octahedral sheet of the silicate layer minus the number of Fe atoms in the hydroxide sheet, was determined to be between 0.5 and 1 from the intensity ratio of the (0 0 3) and (0 0 5) peaks, (Brown and Brindley, 1980). Therefore, the chlorite(s) in SPP1 GWF sediment was relatively rich in Fe, with the Fe located mostly in the silicate sheet.

All reference mineral phases displayed diffraction patterns (Fig. 1) consistent with either the corresponding references (PDF™) (California clinochlore, North Carolina chlorite, Michigan chlorite, SWy-1, Fithian illite, and quartz) or those reported by others (6L-Fh) (Janney et al., 2000, 2001; Kukkadapu et al., 2003; Michel et al., 2007). The Fithian illite contained ~8% quartz based on the XRD peak areas.

Micro-XRD analyses of the mineral slurries were carried out after completion of the uranium adsorption procedure. The analysis revealed no discernible mineral alteration to either the sediment or the reference phases during equilibrium with SGW2. For chlorites, which are unstable mineral phases, ICP analyses of Fe, Al, Si, Mn, Ca, Mg, K and Na (EA-1), indicated that mineral dissolution during the experiment was negligible.

3.1.2. Electron microscopy

SEM analysis of the chlorites and illite revealed the presence of layered, platey microcrystals (e.g. Fig. 2A). The surfaces of larger particles (~15 μm) showed deposits of smaller particles with size ranging from <1 μm to a few microns. The density of the smaller particles varied among the larger particles, and between reference phases. EDS analyses indicated that the major elemental compositions of the reference phases including O, Al, Si, Mg and Fe (EA-2) correlated well with their reported molecular formulas (Table 2). The elemental mapping (see examples in EA-3) revealed uniform elemental distribution throughout the crystallites, except for occasional observations of minor Ti, Mn and/or Ca inclusions in the chlorites. There were no significant differences between compositional measurements made for smaller particles versus larger ones.

The SPP1 GWF, in contrast, was comprised of smaller, nondescript, aggregated particles in the size range of nanometers to a few microns (Fig. 2B). EDS analysis of the bulk sediment was consistent with its high content of basaltic and granitic lithic fragments that are high in Si, Fe, and Ti (Suppplementary EA-4).

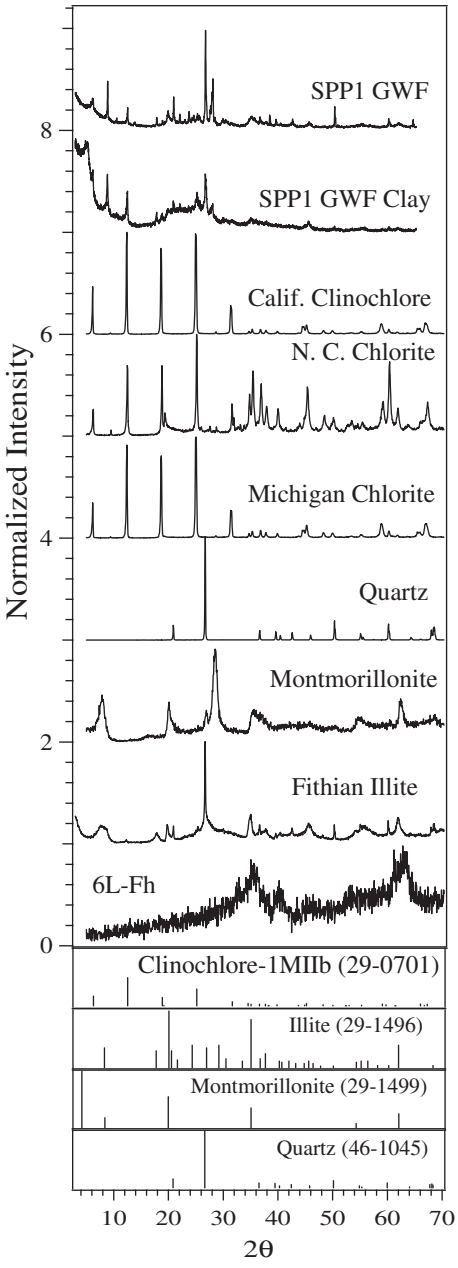

Fig. 1. XRD patterns of SPP1 GWF and reference minerals. The mineral identifications were confirmed by the following standard XRD references: quartz (PDF#01-083-0539); California clinochlore (PDF#00-029-0701); Michigan chlorite (PDF#00-046-1323); North Carolina chlorite (PDF#00-007-0160); illite (PDF#00-026-0911) and montmorillonite, SWy-1, (PDF#29-1499). Some of the PDFs are shown at the bottom. All the XRD patterns were normalized to the same maximum intensity and offset on the intensity axis for clarity.

3.2. U(VI) adsorption

The adsorption of U(VI) on the reference phases ranged between 30.6% on Michigan chlorite to 100% on North

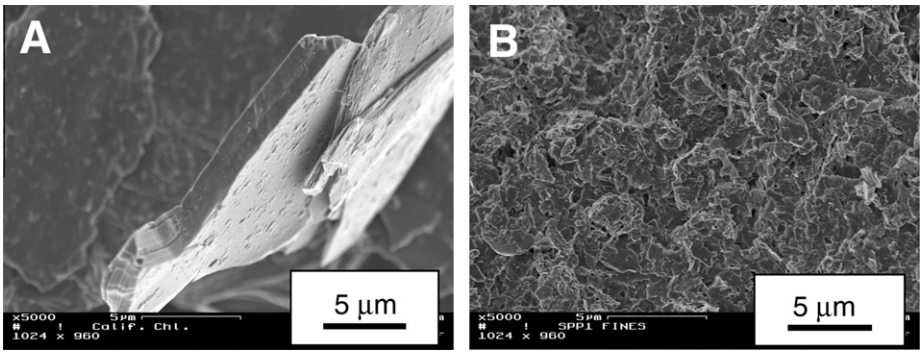

Fig. 2. SEM images of the 5–20 µm fraction of California clinochlore (panel A) and SPP1 GWF (panel B).

Carolina chlorite and 6L-Fh (Table 3). The corresponding U(VI) adsorption K_d values varied with mineral type and the total uranium concentration. The observed K_d values were consistent with those previously reported for ferrihydrite (Waite et al., 1994), montmorillonite (Pabalan and Turner, 1997; Greathouse and Cygan, 2006), quartz (Prikryl et al., 2001), and SPP1 GWF (Bond et al., 2008) under similar experimental conditions. The three chlorites, particularly North Carolina chlorite and California clinochlore, displayed high and variable K_d values. There are no published values for comparison. Among the three chlorites, the K_d decreased with increase in Fe, suggesting that U(VI) was not reduced by structural Fe(II) (e.g. Michigan chlorite).

Normalizing to surface area yielded the following selectivity series for U(VI) adsorption to the reference phases: 6L-Fh > North Carolina chlorite ≈ California clinochlore > quartz ≈ Michigan chlorite > Fithian illite > SWy-1. The surface area normalized K_d decreased with increasing adsorption density (except on North Carolina chlorite), and was lower on silt-sized as compared to the clay-sized fraction of the same adsorbent. SPP1 GWF displayed a low K_d as compared to the reference phases based on the spiked U(VI) alone. However, SPP1 GWF contained 0.13 mmol kg^{-1} of adsorbed contaminant U(VI) (Bond et al., 2008). Consideration of adsorbed contaminant U(VI) yielded larger surface area normalized K_d values (6.35 and 1.29 mL m^{-2}). These larger values were comparable to those on some of the phyllosilicates (Table 3), and to those reported for sediments with similar mineralogical and solution conditions (Curtis et al., 2006; Um et al., 2007; Zachara et al., 2007; Bond et al., 2008).

3.3. Fluorescence spectra of U(VI)

The fluorescence spectra of U(VI) adsorbed on the reference minerals displayed characteristic patterns (Fig. 3 traces a–g and Table 4). The first spectral pattern, appearing on quartz (Fig. 3 trace a), consisted of a significantly weaker first vibronic band at ~481 nm followed by overlapping bands at 498.6, 519.7 and 541.0 nm. The second spectral pattern, appeared on SWy−1, North Carolina chlorite, California clinochlore and Fithian illite; and consisted of a much stronger first band at ~481 nm followed by a set of almost evenly spaced bands at ~501, 522 and 544 nm

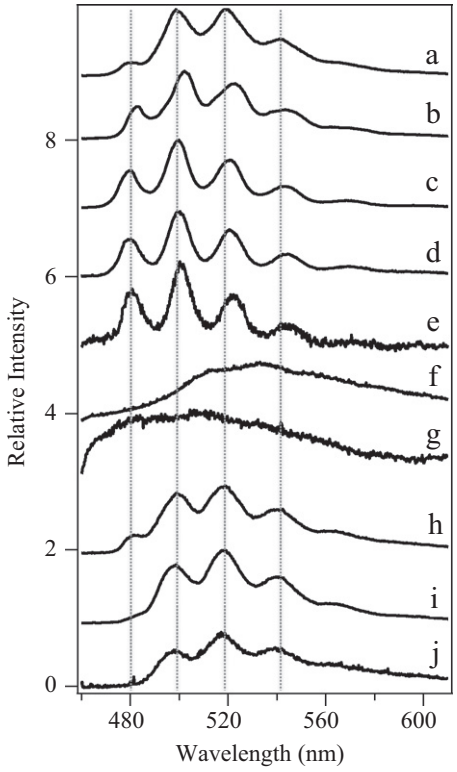

Fig. 3. LHeT Fluorescence spectra of U(VI) adsorbed on SPP1 GWF and the reference minerals: (a) Quartz (4.50); (b) Fithian illite (<2 um fraction) (2.53); (c) SWy-1 (44); (d) California clinochlore (5–20 µm fraction) (0.70); (e) North Carolina chlorite (2–5 µm fraction) (0.11); (f) 6L-Fh (0.30); and (g) Michigan chlorite (2–5 µm fraction) (0.06); (h) SPP1 GW fines (1.00); (i) SPP1 GW fines without addition of U(VI) solution and (j) the ⩽53 µm fraction of a sediment sample retrieved from the nearby north infiltration pond at a depth of 16 ft below ground surface. All spectra were normalized to the same maximum intensity (data in parenthesis indicate relative intensity) and offset along the *Y*-axis. $\lambda_{ex} = 415$ nm.

(Fig. 3 traces b–e). The third spectral pattern included 6L-Fh and Michigan chlorite, which showed weak and unresolved spectra that were red-shifted relative to the others (Fig. 3f and g). Both 6L-Fh and Michigan chlorite contain high Fe. Thus the weak, poorly-resolved spectra likely

Table 4
Fluorescence spectral characteristics of adsorbed U(VI) at liquid helium temperature. $\lambda_{ex} = 415$ nm.

Mineral	Spectral maxima (nm)	No. species	ν_1(f) (cm^{-1})	τ (μs)
Montmorillonite	479.9, 499.9, 520.1, 541.4	2	7891	656, 105
Fithian illite (<2 μm)	482.4, 502.1, 521.8, 543.7, 570.2	2	797	19
Michigan chlorite (2–5 μm)	512.3, 532.0, 561.0	–	815	24
Michigan chlorite (5–20 μm)	—*	–	–	23
N.C. chlorite (2–5 μm)	481.1, 501.6, 522.1, 544.3	1	804	22
N.C. chlorite (5–20 μm)	481.1, 502.2, 521.9, 544.3	1	804	23
Cal. clinochlore (2–5 μm)	481.1, 501.4, 521.9, 544.3	1	804	28
Cal. clinochlore (5–20 μm)	478.9, 500.3, 520.5, 544.3, 569.4	1	836	–
Quartz (5–30 μm)	498.6, 519.7, 541.0	2	779	459, 21
6L-Fh	511.2, 536.0, 556.9	–	815	31
SPP1 GWF	498.6, 519.7, 542.1, 564.5	2	779	212, 21
$M_xUO_2(CO_3)_3^{2x-4}$ (aq) (M = Ca, Mg; $x = 1, 2$)	481.4, 501.6, 522.1, 545.4	1	812	1121

resulted from fluorescence quenching by Fe (Stepanov et al., 1984).

The fluorescence spectra of spiked U(VI) adsorbed on SPP1 GWF (Fig. 3 trace h) displayed a weak band at 481.0 nm followed by strong bands at 498.6, 519.7, 542.1 and 564.5 nm. These features were identical to those for the contaminated sediment (0.13 mmol kg^{-1} U) that was not contacted with additional U(VI) (Fig. 3 trace i). Another contaminated vadose zone sediment (<53 μm fraction NPP1-16; 0.04 mmol kg^{-1} U) also showed a similar spectra (Fig. 3 trace j). This spectrum motif therefore appears characteristic of low concentration adsorbed U(VI) in the 300 area vadose and saturated zones.

The time-resolved fluorescence spectral profiles for SWy-1, North Carolina chlorite and California clinochlore remained similar at different delay times (data not shown), suggesting that a single dominant environment exists for adsorbed U(VI) on each phase. The U(VI) fluorescence decay curves for these phases were best fit by a single exponential function, except for SWy-1 (Table 4). However, for quartz, Fithian illite and SPP1 GWF, the band at ca. 481 nm gained intensity (Fig. 4) as the delay time increased. The spectra of uranyl species are typically composed of a series of four to six nearly evenly-spaced vibronic bands in the visible range. Thus, additional bands at longer wavelengths that were not resolved from the existing intense bands must also have gained intensity along with the 481 nm band. For Fithian illite, this became obvious at delay times greater than 20 μs (Fig. 4c). A set of well-resolved bands appeared and remained invariant at delay times greater than 400 μs,, indicating the presence of a unique surface U(VI) species.

The time-resolved spectra for Fithian illite could be simulated by the linear combination of two spectral profiles representing unique species (Fig. 5). The vibronic bands of the first U(VI) species were located at 482.7, 502.7, 523.7, 546.7 and 573.5 nm while those of the second

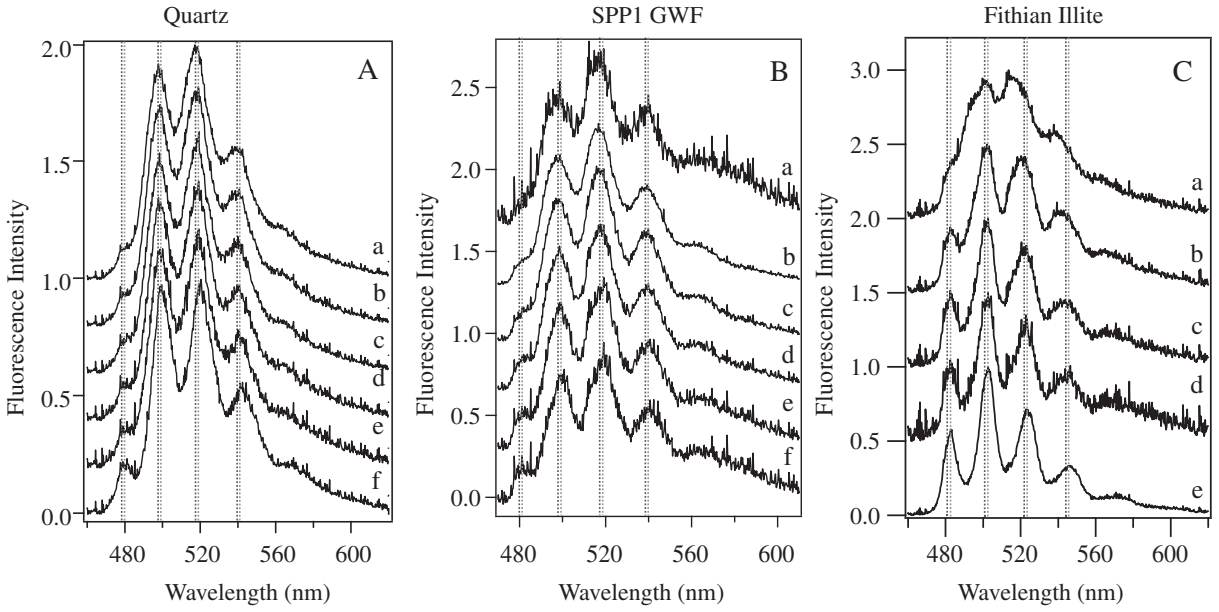

Fig. 4. Time-resolved fluorescence spectra of U(VI) adsorbed on quartz (A), SPP1 GWF (B) and Fithian illite (C). In (A), the delay times were (a) 0 μs; (b) 50 μs; (c) 100 μs; (d) 200 μs; (e) 300 μs; (f) 800 μs and time gate was maintained at 100 μs. In (B), the delay times were (a) 0 μs (gate width 10 μs); (b) 0 μs; (c) 50 μs; (d) 80 μs; (e) 180 μs; (f) 280 μs and time gate was maintained at 100 μs except (a); In (C), the delay times were (a) 0 μs (gate width 5 μs); (b) 0 μs; (c) 100 μs; (d) 200 μs and (e) 400 μs (gate width 0.5 ms). For (b–d), the gate width was 20 μs. All spectra were normalized to the same maximum intensity and offset along the Y-axis. $\lambda_{ex} = 415$ nm.

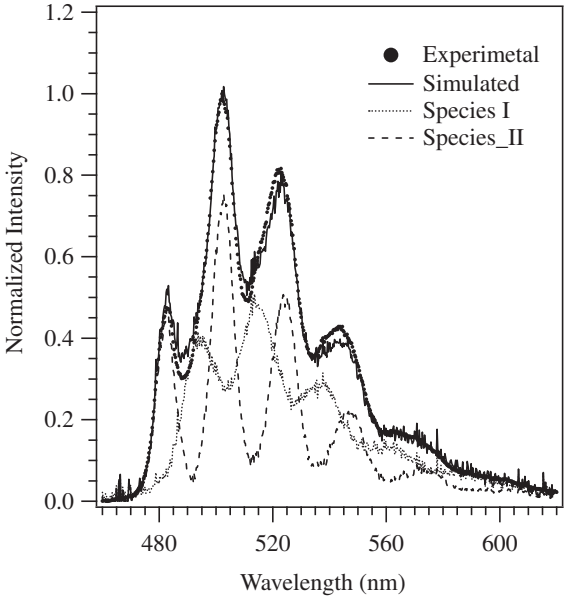

Fig. 5. Deconvolution of the fluorescence spectra of U(VI) on Fithian illite into two spectral components.

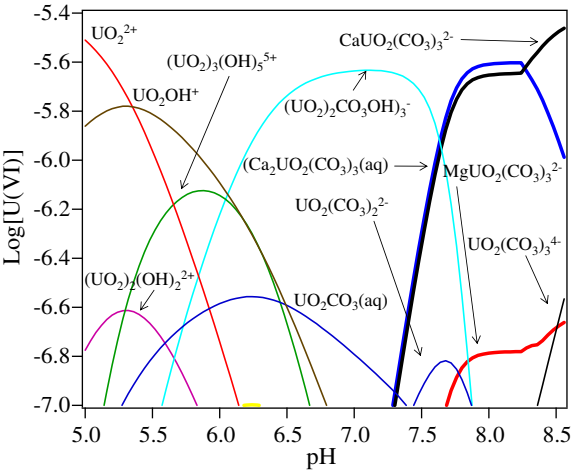

Fig. 7. U(VI) speciation in SGW2. $[U(VI)_{Total} = 5 \times 10^{-6}$ mol L^{-1}. pH 8.1. $P_{CO_2} = = 10^{-3.5}$ atm. In the diagram: (a) UO_2^{2+}; (b) UO_2OH^+; (c) $(UO_2)_2(OH)_2^{2+}$; (d) $(UO_2)_3(OH)_5^+$; (e) UO_2CO_3(aq); (f) $(UO_2)_2CO_3(OH)_3^-$; (g) $UO_2(CO_3)_2^{2-}$; (h) $Ca_2UO_2(CO_3)_3$(aq); (i) $CaUO_2(CO_3)_3^{2-}$; (j) $MgUO_2(CO_3)_3^{2-}$ and (k) $UO_2(CO_3)_3^{4-}$.

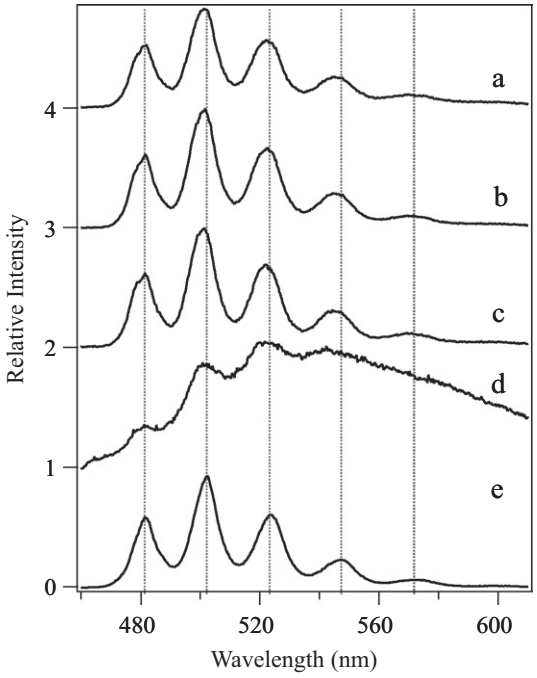

Fig. 6. LHeT fluorescence spectra of U(VI) in the supernatants after equilibration with adsorbents. (a) U(VI) in SGW2; (b) SPP1 GWFs; (c) quartz; (d) 6L-Fh and (e) $Ca_2UO_2(CO_3)_3$ (aq). All spectra were normalized to the same maximum intensity and offset along the *Y*-axis. $\lambda_{ex} = 415$ nm.

U(VI) species were at 494.5, 513.6, 537.7 and 562.6 nm. Consistent with the time-resolved spectra, the fit of the fluorescence decay curves required two exponentials (Table 4). The spectral characteristics of the first species were consistent with those in montmorillonite and chlorites. The spectral profile of the second species was similar to that of U(VI) adsorbed on quartz, although the peak positions did not exactly match. Considering that the Fithian illite contained ~8% quartz, it is logical to conclude that the second species was due to U(VI) sorption on quartz. The small deviation of the peak positions could be due to errors in the spectral analysis, or from the specific properties of impurity quartz in Fithian illite.

U(VI) fluorescence spectra were also recorded for the adsorption experiment supernatants, and for SGW2 that was spiked with U(VI) nitrate. These all showed similar fluorescence spectra (Fig. 6) with U(VI) vibronic bands located at 481.4, 501.4, 522.7, 545.4 and 571.6 nm, and average peak spacing of ~820 cm^{-1}. The aqueous phase spectral characteristics were similar to those of the dicalcium U(VI) tricarbonate complex (Fig. 6e), in accord with aqueous speciation calculations where $Ca_2UO_2(CO_3)_3$(aq) and $CaUO_2(CO_3)_3^{2-}$ were the dominant aqueous U(VI) species in SGW2 (Fig. 7).

3.4. Chemometric analysis

The noise-reduced fluorescence spectra for all the samples (EA-5) were only marginally different from the original spectra (Fig. 3), an indication of the high quality of the spectral measurements. The existence of a weaker second spectral component in SPP1 GWF was clearly revealed on the asynchronous correlation plot of the noise-reduced spectra collected at different time delays and U(VI) concentrations (Fig. 8). This plot showed the presence of peaks centered at 480, 491, 500, 513, 522, 537 and 560 nm (Fig. 8). Among these peaks, the 500 and 513 nm bands form clear asynchronous correlation squares and therefore indicate that they arise from different U(VI) species as reflected by their color schemes. The 500 and 522 nm bands also form asynchronous correlation squares with the 537

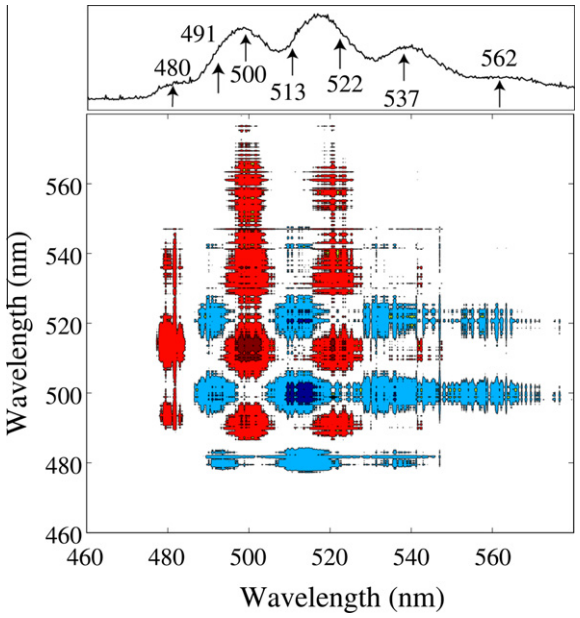

Fig. 8. Asynchronous 2D correlation map of SPP1 GWFs at different delay times. The red and blue cross-peaks underscore the presence of two distinct collections of vibronic peaks with different temporal fluorescence behaviors. (For interpretation of the references to color in this figure legend, the reader is referred to the web version of this article.)

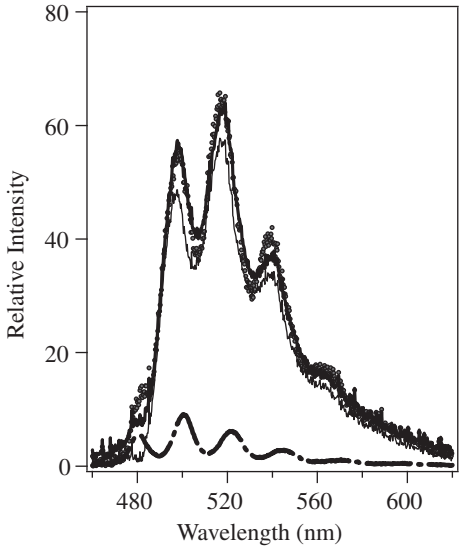

Fig. 9. Simulation (□) of the fluorescence spectra of U(VI) adsorbed on SPP1 GWF (···) by a linear combination of the spectra of U(VI) on quartz (—) and California clinochlore (– - –).

and 560 nm bands while they form no such squares with the 480 nm peak. On the other hand, the 491 and 513 nm peaks form asynchronous correlation squares with the 480 nm band. These correlations provided evidence for two distinct spectral components of adsorbed U(VI) with positions at 480, 500 and 522 nm for the first species; and 491, 513, 537 and 560 nm for the second.

The same analysis was also performed for U(VI) adsorbed on quartz and all the phyllosilicate reference minerals (data not shown). Similar results to those of SPP1 GWF were obtained for quartz and Fithian illite, indicating the presence of two U(VI) species on each of these phases. For Fithian illite, the species with peak positions of 480, 500 and 522 nm, which corresponded to the weaker spectral component in SPP1 GWF and quartz, became dominant in all the spectra with time delays greater than 100 μs, consistent with the analysis of time-resolved spectra indicating that this U(VI) species had a longer fluorescence lifetime. For North Carolina chlorite, California clinochlore, and SWy-1, there was only one dominant U(VI) species. These results were consistent with the observations from the time-resolved spectra (Fig. 4). It was assumed that the 6L-Fh and Michigan chlorite did not contribute to the spectra of U(VI) adsorbed on SPP1 GWF because of their obvious dissimilarity. It was not possible to determine whether these phases were significant adsorbents of U(VI) in the sediment because of strong fluorescence quenching.

The spectra of the dominant U(VI) spectral component in SPP1 GWF closely resembled that in quartz and the Fithian illite at shorter delay times. The spectra of the second U(VI) component in SPP1 GWF was similar to that of California clinochlore, North Carolina chlorite and SWy−1 (Figs. 3 and 5). The latter component also appeared in the U(VI)-spiked SGW2 sample, in which the $Ca_2UO_2(CO_3)_3$(aq) species dominated (Figs. 6, 7). This similarity underscores the highly similar coordination environments for U(VI) in both the aqueous phase and at the phyllosilicate mineral interface.

The spectra of adsorbed U(VI) on SPP1 GWF was simulated by a linear combination of the U(VI) spectra for quartz (90%) and for the phyllosilicates (10%) (Fig. 9). The goodness of fit using spectra from any of the four phyllosilicates was similar. Including U(VI) spectra from more than one phyllosilicate did not improve the fit because the spectral characteristics of adsorbed U(VI) on California clinochlore, SWy-1, and North Carolina chlorite were similar.

The above results were based on the normalized fluorescence spectra. Determination of the concentration of the two U(VI) surface species requires knowledge of their quantum yields as well as fluorescence quenching effects in the sediment. These data are not currently available. Therefore, the actual concentration ratio of the quartz and phyllosilicate U(VI) species may be different from the 9:1 ratio obtained from the spectral simulations. Considering that the relative fluorescence intensities for U(VI) adsorbed on quartz and California clinochlore (clay fraction) was 4.5:0.11 (Fig. 3 caption), it is probable that the concentration of phyllosilicate-adsorbed U(VI) in the sediment was significantly higher than that reflected by the 9:1 ratio.

4. DISCUSSION

4.1. U(VI) adsorption affinity on reference minerals

The measured U(VI) adsorption K_d values (Table 3) compare favorably with those reported previously on quartz (Prikryl et al., 2001), montmorillonite (Pabalan

and Turner, 1997) and Fe-oxyhydroxide (Hsi and Langmuir, 1985) under similar experimental conditions. Differences in U(VI) adsorption extent to quartz and ferrihydrite as compared to the results of Fox et al. (2006) were noted that result from solid–liquid ratio effects. Direct comparisons are not easily made with other previous studies of U(VI) adsorption to smectites (Chisholm-Brause et al., 1994; Morris et al., 1994; McKinley et al., 1995; Turner et al., 1996; Sylwester et al., 2000; Chisholm-Brause et al., 2001; Hennig et al., 2002; Chisholm-Brause et al., 2004; Kowal-Fouchard et al., 2004; Catalano and Brown, 2005) and quartz or amorphous silica (Glinka et al., 1997; Arnold et al., 1998; Gabriel et al., 2001; Froideval et al., 2003) because of differences in solution pH, U(VI) concentration, solid-to-liquid ratio, and carbonate concentration as well as the procedure of mineral preparation.

U(VI) affinity varied by more than two orders of magnitude for the phyllosilicates with the highest K_d values observed for chlorites, particularly the ones rich in Mg but poor in Fe (Table 3). The high affinity of U(VI) on chlorites was consistent with the observation of nearly complete adsorptive removal of U(VI) by ripidolite, a Fe-rich chlorite, at pH 6.5 by Singer et al. (2009a), and the sequential extraction results of Baik et al. (2004) that implied that chlorite was a strong U(VI) adsorbent in crushed granite. The mechanisms of U(VI) sorption on chlorite are poorly understood, specifically the relative roles of surface complexation versus reduction. EXAFS results suggested that U(VI) adsorption to Fe-rich ripidolite occurred by surface complexation with [$Fe(O,OH)_6$] octahedral sites (Singer et al., 2009a) without valence change. However, the present results indicated that U(VI) adsorption on Mg-rich/Fe-poor chlorites was stronger than Fe-rich Michigan chlorite. Further research is needed to explain such adsorption behavior.

The large range in surface area-normalized K_d values among the reference phases indicated that some of these may be important U(VI) sorbents when they are present at low mass% (e.g. ferrihydrite and Mg chlorite) while others, including smectite and quartz, require sizable concentration for impact.

4.2. Mineralogical association of U(VI) in SPP1 GWF

The chemometric analysis indicated that the fluorescence-active component of adsorbed U(VI) was associated with quartz and phyllosilicates. Such a conclusion was consistent with the quartz- and phyllosilicate-rich mineralogy of the contaminated sediment; the relatively low measured K_d values for the sediment, quartz, and some of the phyllosilicates (montmorillonite and illite, primarily); and with previously reported trends of U(VI) speciation in the Hanford 300A vadose zone. Highly contaminated sediments existed at the top of the vadose zone profile where U(VI) was incorporated into calcite and aragonite, and other U(VI) oxyhydroxide precipitates (Wang et al., 2004a). U(VI) phosphate precipitates, such as metatorbernite and others, were observed at intermediate vadose zone depths (Catalano et al., 2006; Arai et al., 2007; Stubbs et al., 2009). Adsorption complexes on phyllosilicates were believed to dominate in the deeper vadose zone and aquifer sediments based on EXAFS analyses (Catalano et al., 2006; Arai et al., 2007; Singer et al., 2009b), but signal strength was too low for quantitative analysis.

The present results provide the first documentation of the importance of quartz to U(VI) adsorption in Hanford 300 area sediment. This finding was unexpected but supported by spectroscopic measurement. As the single, most abundant sediment mineral, the large contribution of quartz could result from its relatively high affinity for U(VI) as reflected by the high surface area normalized K_d values, and high surface area resulting from its presence as a mass dominant mineral phase in all size fractions, e.g. sand, silt and clay (Fig. 1). Aside from quartz, amorphous silica resulting from basalt comminution is an abundant non-crystalline phase in the sediment. U(VI) adsorbed on amorphous silica will display the same spectral signatures as U(VI) adsorbed on quartz. Strong U(VI) adsorption on quartz in near-neutral solution was reported by Kohler et al. (1996) in systems containing 1×10^{-6} mol L^{-1} U(VI) and 100 g/L of quartz. U(VI) adsorption increased as a function of pH and reached nearly 100% at pH 7 even in the presence of 5×10^{-4} mol L^{-1} fluoride. Similarly, Gabriel et al. (2001) observed that U(VI) (1×10^{-6} mol L^{-1}) was strongly adsorbed by quartz between pH 5.5 and 8.5.

Surface complexation modeling (SCM) was performed to calculate the U(VI) adsorption K_d values for reference quartz and for SPP1 GWF by assuming that 50% of the sand and silt fractions in SPP1 GWF was comprised of quartz. A non-electrical SCM (Davis, 2001) was used in model calculations (See EA-6 for modeling parameters). The calculated K_d values for the quartz reference were 13.7 and 12.1 mL g^{-1} at U(VI) concentrations of 5×10^{-7} and 5×10^{-6} mol L^{-1}, respectively, consistent with those measured (Table 3). Assuming that the quartz in SPP1 GWF has the same adsorption site density (0.356 μmoL g^{-2}) and surface area (0.33 m^2 g^{-1}) as those for reference quartz, the calculated K_d values for SPP1 GWF were 6.1 and 5.4 mL g^{-1} at total U(VI) concentrations of 5×10^{-7} and 5×10^{-6} mol L^{-1}, respectively, with respect to the mass of the sediment. If the quartz in SPP1 GWF was assumed to have the same site density as the reference quartz (0.356 mol m^{-2}), but exhibit a surface area equal to the silt–sand fractions in SPP1 GWF, 53.0 m^2 g^{-1} (EA-6), the calculated K_d values reach 1.14×10^3 mL g^{-1} for both U(VI) concentrations of 5×10^{-7} and 5×10^{-6} mol L^{-1}. The much higher calculated K_d for the latter scenario was due to the high surface area. In either case, the calculated K_d values were significant compared to those measured for SPP1 GWF, offering further support for a significant contribution of quartz to U(VI) adsorption in the sediment.

A concern for the proposed speciation model is the inadvertent exclusion of the contribution of U(VI) adsorption on Fe(III)-oxide because of its strong fluorescence quenching effect. Fe(III) oxides are well-known for their high adsorption affinity for U(VI) in neutral to weakly basic solutions (Hsi and Langmuir, 1985; Waite et al., 1994; Payne et al., 1996; Hiemstra et al., 2009). We expected these

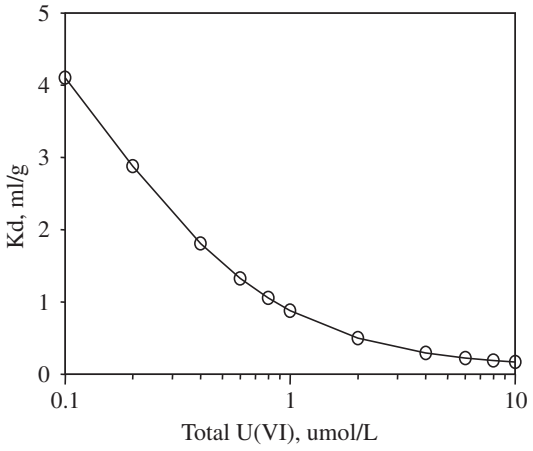

Fig. 10. Calculated U(VI) K_d (mL/g) from the ferrihydrite model. The conditions are: solid:water ratio = 15 g L^{-1}; [ferrihydrite Fe] = 9×10^{-5} mol L^{-1}. The calculated dominant aqueous species are $Ca_2UO_2(CO_3)_3$ (aq) and $CaUO_2(CO_3)_3^{2-}$.

phases to be important here, existing as weathering products of ubiquitous Fe(II)-containing lithogenic phases in basalt and granitic lithic fragments that dominate the host sediment. Arnold et al. (2001), for example, observed that a small amount of ferrihydrite derived from chlorite weathering was the dominant adsorbent in phyllite. While XRD analysis showed no detectable crystalline Fe oxides in SPP1 GWF (Fig. 1), EDS analysis revealed discrete Fe mineral phases at some spots (EA-4). The SPP1 GWF contains 0.5% hydroxylamine hydrochloride (HAHC) extractable, poorly crystalline Fe(III) oxide and 1.3% dithionite-citrate-bicarbonate extractable crystalline Fe(III) oxides (Bond et al., 2008). To evaluate whether ferrihydrite might be an important adsorbent, U(VI) sorption K_d values were calculated based on the HAHC Fe concentration using an existing surface complexation model (Waite et al., 1994; Liu et al., 2005) under the present experimental conditions (See EA-7 for model parameters). The results (Fig. 10) showed that the HAHC Fe will result in K_d values of only 0.25 and 1.5 mL g^{-1} with respect to sediment mass at total U(VI) concentrations of 5×10^{-6} and 5×10^{-7} mol L^{-1}, respectively. The contribution of poorly crystalline Fe(III) oxides to U(VI) adsorption in SPP1 GWF is, consequently, likely to be small.

4.3. U(VI) surface species

U(VI) adsorption on most mineral phases occurs through formation of inner-sphere surface complexes above pH 6 (McKinley et al., 1995; Bond et al., 2008; Sherman et al., 2008; Hiemstra et al., 2009). For quartz, Fe(III)-oxides and phyllosilicates, the inner-sphere complexation sites are surface oxygens and hydroxylated surface sites such as silanols, aluminols and ferrinols.

Inner-sphere U(VI) complexes with deprotonated silanols under near-neutral conditions have been identified on quartz by multiple methods (Waite et al., 1994; Reich et al., 1996; Sylwester et al., 2000; Gabriel et al., 2001). In the presence of atmospheric CO_2, Gabriel et al. (2001) identified three surface complexes on amorphous silica: $\equiv SiO_2UO_2^0$ with a fluorescence lifetime of 170 ± 25 μs that appeared between pH 4 and 7, $\equiv SiO_2UO_2OH^-$ with a fluorescence lifetime of 360 ± 50 μs dominated between pH 6.5 and 8.5, and a non-fluorescent ternary uranyl–silica–carbonate surface complex, $\equiv SiO_2UO_2OHCO_3^{3-}$, that was present between pH 8–9. The fluorescence spectra of U(VI) adsorbed on quartz in this work (Fig. 3a) closely resembled the $\equiv SiO_2UO_2OH^-$ complex on amorphous silica (Gabriel et al., 2001). At LHeT, the ternary complex $\equiv SiO_2UO_2OHCO_3^{3-}$ may fluoresce too. However, its spectrum is unknown. Further examination of the fluorescence peak spacings (v_1 values in Table 2) revealed that the v_1 value for U(VI) adsorbed on quartz was 779 cm^{-1}. Such a v_1 value is typical for U(VI) silicate minerals (Wang et al., 2008), providing additional evidence for inner-sphere U(VI) complexation with deprotonated surface silanol groups.

The adsorption of U(VI) to phyllosilicates occurs on amphoteric edge sites in weakly basic solutions (Zachara and McKinley, 1993a; Chisholm-Brause et al., 1994; McKinley et al., 1995; Giaquinta et al., 1997; Chisholm-Brause et al., 2004; Catalano and Brown, 2005; Arnold et al., 2006). The edge sites include the silanol groups, aluminol groups, Al–O–Si bridging oxygen sites as well as sites involving other metal substitutions such as Fe and Mg. The brucite layer on chlorites, (often with further Mg-substitutions by Fe and Al, etc.) offers additional potential U(VI) binding sites.

The fluorescence spectra of U(VI) adsorbed on phyllosilicates (Fig. 3 traces b–e) were nearly identical to those of U(VI) in SGW2 and supernatants of the adsorption samples (Fig. 6). Thes spectral profiles match well with that of uranyl-tricarbonate complexes (Wang et al., 2004b), consistent with the results of thermodynamic calculations for SGW2 at pH 8.1 [$(Ca_2UO_2(CO_3)_3^0$ (49.7%), $CaUO_2(CO_3)_3^{2-}$ (45.0%), $MgUO_2(CO_3)_3^{2-}$ (3.3%), $UO_2(CO_3)_3^{4-}$ (0.8%) and $UO_2(CO_3)_2^{2-}$ (1.1%)]. Since the supernatants in both North Carolina chlorite and California clinochlore showed no fluorescence (data not shown) because of high fractional U(VI) adsorption, the observed spectra were not due to residue supernatant in the solid paste. We therefore concluded that the fluorescence spectra of U(VI) adsorbed on phyllosilicates resulted from U(VI) tricarbonate-type surface complexes.

Uranyl-tricarbonate surface complexes have been reported by others (Elzinga et al., 2004; Hiemstra et al., 2009). EXAFS and luminescence spectroscopy indicated the formation of uranyl tricarbonate-like surface complexes on calcite at pH 7.4 and 8.3 with low U(VI) concentrations ($<5 \times 10^{-4}$ mol L^{-1}) (Elzinga et al., 2004). A U(VI) tricarbonate surface complex, $\equiv(UO_2)(CO_3)_3^{4-}$, forms on ferrihydrite and becomes the most abundant U(VI) species at high pH and carbonate concentrations (Hiemstra et al., 2009). The surface complex is singly-coordinated to structural Fe via a carbonate group. The bonding nature of U(VI)–tricarbonate complexation on the phyllosilicate surface is not yet understood. The high K_d values observed for the Fe-poor chlorites suggest involvement of the brucite layer.

5. IMPLICATIONS

Two common surface complexation modeling approaches are used for metal adsorption on natural mineral assemblages: (i) the generalized composite model (GC) where generic surface sites are assumed for the entire mineral assemblage, and (ii) the component additivity model (CA) where adsorption is described as the sum of that occurring on individual mineral phases (Davis et al., 1998). The GC approach is most commonly taken because of difficulties in determining speciation, reactive mineral surface areas, and individual mineral concentrations and surface complexation parameters in heterogeneous sediments. However, the fact that the U(VI) fluorescence spectra on SPP1 GWF could be effectively simulated as a linear combination of the spectra of U(VI) adsorbed on quartz and phyllosilicates implied that the CA model might be a workable approach in this case. Yet, the consistently smaller surface area normalized K_d values for the sediment as compared to the reference phases suggested that such "addition" is not a simple task. Sediment surface properties depend on the aggregation state of the reactive particles, and *in situ* chemical conditions that modify available site concentrations, affinities, and speciation in complex ways. Consequently, adjustment of the surface site densities, reactive surface area, and/or surface complex stability constants for the individual phases may be necessary to adequately describe adsorption in the sediment. For fluorescence-based measurement, the determination of the true concentration distribution of U(VI) adsorption complexes on the contributing phases requires knowledge of the quantum yields of the surface complexes and the quenching effect of the mineral host.

Phyllosilicates are important in U(VI) adsorption and retention in most subsurface sediments containing a measurable silt and clay content. The similar, uranyl-tricarbonate-like spectra on the different phyllosilicates studied suggest a common type of surface U(VI) adsorption site in weakly basic groundwater. While this may simplify surface complexation models, it makes quantification of the contribution of individual phyllosilicate phases a difficult task, especially where they exhibit high variability for U(VI) adsorption (Table 3). Ample evidence indicate that small fractions of chlorites, along with usually higher levels of smectites and illites, are present at many contamination sites (Serne et al., 2002; Davis and Curtis, 2003; Zachara et al., 2005, 2007). The high affinity of chlorite and its weathering products, such as ferrihydrite, for U(VI) implies that chlorites and associated phases may play important but as yet undocumented roles in U(VI) adsorption in the field. The present results also indicate that U(VI)–tricarbonate complexes, the major aqueous species in most environmental waters, require explicit consideration in the modeling of U(VI) surface complexation on phyllosilicates.

ACKNOWLEDGEMENTS

The authors thank Drs. Ponnusamy Nachimuthu and Mark Bowden at the W.R. Wiley Environmental Molecular Sciences Laboratory (EMSL), Mr. Todd Schaef, Dr. Igor Kutnyakov and Ms. Colleen Russell for XRD analysis of the solids, and Mr. Bruce Arey (EMSL) for SEM and EDAX analysis. We also thank Dr. Eugene Ilton for helpful discussions and reviewing the manuscript. This project was supported by the Subsurface Biogeochemistry Research Program (SBR) managed by the U.S. DOE Office of Biological and Environmental Research (OBER) through the Pacific Northwest National Laboratory (PNNL) Scientific Focus Area (SFA). Part of this research was performed at EMSL, a national scientific user facility at PNNL managed by the Department of Energy's Office of Biological and Environmental Research. Pacific Northwest National Laboratory is operated for the US Department of Energy by Battelle under Contract DE-AC06-76RLO 1830.

APPENDIX A. SUPPLEMENTARY DATA

Supplementary data associated with this article can be found, in the online version, at doi:10.1016/j.gca.2011.03.008.

REFERENCES

Allison J. D., Brown D. S. and Novo-Gradac K. J. (1998) *MINTEQA2/PRODEFA2, a geochemical assessment model for environmental systems (version 4)*. Environmental Research Laboratory, U.S. EPA.

Arai Y., Marcus M. K., Tamura N., Davis J. A. and Zachara J. M. (2007) Spectroscopic evidence for uranium bearing precipitates in vadose zone sediments at the Hanford 300-area site. *Environ. Sci. Technol.* **41**(13), 4633–4639.

Arai Y., McBeath M., Bargar J. R., Joye J. and Davis J. A. (2006) Uranyl adsorption and surface speciation at the imogolite-water interface. Self-consistent spectroscopic and surface complexation models. *Geochim. Cosmochim. Acta* **70**(10), 2492–2509.

Arnold T., Utsunomiya S., Geipel G., Ewing R. C., Baumann N. and Brendler V. (2006) Adsorbed U(VI) surface species on muscovite identified by laser fluorescence spectroscopy and transmission electron microscopy. *Environ. Sci. Technol.* **40**(15), 4646–4652.

Arnold T., Zorn T., Bernhard G. and Nitsche H. (1998) Sorption of uranium(VI) onto phyllite. *Chem. Geol.* **151**(1–4), 129–141.

Arnold T., Zorn T., Zanker H., Bernhard G. and Nitsche H. (2001) Sorption behavior of U(VI) on phyllite: experiments and modeling. *J. Contam. Hydrol.* **47**(2–4), 219–231.

Baik M. H., Hyun S. P., Cho W. J. and Hahn P. S. (2004) Contribution of minerals to the sorption of U(VI) on granite. *Radiochim. Acta* **92**(9–11), 663–669.

Bargar J. R., Reitmeyer R. and Davis J. A. (1999) Spectroscopic confirmation of uranium(VI) – carbonato adsorption complexes on hematite. *Environ. Sci. Technol.* **33**, 2481–2484.

Barnett M. O., Jardine P. M. and Brooks S. C. (2002) U(VI) adsorption to heterogeneous subsurface media: application of a surface complexation model. *Environ. Sci. Technol.* **36**, 937–942.

Bernhard G., Geipel G., Brendler V. and Nitsche H. (1998) Uranium speciation in waters of different uranium mining areas. *J. Alloy Compds.* **271–273**, 201–205.

Bond D. L., Davis J. A. and Zachara J. M. (2008) Uranium(VI) release from contaminated vadose zone sediments: estimation of potential contributions from dissolution and desorption. In *Developments in Earth and Environmental Sciences*, vol. 7 (ed. O. B. A. D. B. K. Mark), pp. 375–416. Developments in Earth and Environmental Sciences. Elsevier.

Brown, G. and Brindley, G. W. (1980) X-ray diffraction procedures for clay mineral identification. In (G. W. Brindley and G. Brown eds.), *Crystal Structure of Clay Minerals and Their X-Ray Identification*. London, Mineralogical Society, Monograph 5.

Catalano J. G. and Brown J. G. E. (2005) Uranyl adsorption onto montmorillonite: evaluation of binding sites and carbonate complexation. *Geochim. Cosmochim. Acta* **69**(12), 2995–3005.

Catalano J. G., McKinely J. P., Zachara J. M., Heald S. M., Smith S. C. and Brown, Jr., G. E. (2006) Changes in uranium speciation through a depth sequence of contaminated Hanford sediments. *Environ. Sci. Technol.* **40**(8), 2517–2524.

Chang H.-S., Korshin G. V., Wang Z. and Zachara J. M. (2006) Adsorption of uranyl on gibbsite: a time-resolved laser-induced fluorescence spectroscopy (TRLIFS) study. *Environ. Sci. Technol.* **40**, 1244–1249.

Chisholm-Brause C., Conradson S. D., Buscher C. T., Eller P. G. and Morris D. E. (1994) Speciation of uranyl sorbed at multiple binding-sites on montmorillonite. *Geochim. Cosmochim. Acta* **58**(17), 3625–3631.

Chisholm-Brause C. J., Berg J. M., Little K. M., Matzner R. A. and Morris D. E. (2004) Uranyl sorption by smectites: spectroscopic assessment of thermodynamic modeling. *J. Colloid Interf. Sci.* **277**, 366–382.

Chisholm-Brause C. J., Berg J. M., Matzner R. A. and Morris D. E. (2001) Uranium(VI) sorption complexes on montmorillonite as a function of solution chemistry. *J. Colloid Interf. Sci.* **233**, 38–49.

Curtis, G. P., Davis, J. A. and Naftz, D. L. (2006) Simulation of reactive transport of uranium(VI) in groundwater with variable chemical conditions. *Water Resour. Res.* **42**(4).

Davis, J. and Curtis, G. (2003) Application of surface complexation modeling to describe uranium (VI) adsorption and retardation at the uranium mill. tailings site at Naturita, Colorado,. *NUREG Report CR-6820,* Washington, DC, U. S. Nuclear Regulatory Commission.

Davis, J. A. (2001). Surface Complexation Modeling of Uranium(VI) Adsorption on Natural Mineral Assemblages. Washington, DC 20555-0001, US Geological Survey.

Davis J. A., Coston J. A., Kent D. B. and Fuller C. C. (1998) Application of surface complexation concept to complex mineral assemblages. *Environ. Sci. Technol.* **32**, 2820–2828.

DOE (1995). The DOE National 1995 Mixed Waste Inventory Report.

DOE (2001). Summary Data on the Radioactive Waste, Spent Nuclear Fuel, and Contaminated Media managed by the U.S. Department of Energy, April 1, 2001.

Drever J. I. (1973) Preparation of oriented clay mineral specimens for X-ray-diffraction analysis by a filter-membrane peel technique. *Am. Mineral.* **58**(5–6), 553–554.

Duff M. C., Coughlin J. U. and Hunter D. B. (2002) Uranium coprecipitation with iron oxide minerals. *Geochim. Cosmochim. Acta* **66**(20), 3533–3547.

Duff M. C., Morris D. E., Hunter D. B. and Bertsch P. M. (2000) Spectroscopic characterization of uranium in evaporation basin sediments. *Geochim. Cosmochim. Acta* **64**(9), 1535–1550.

Elzinga E. J., Tait C. D., Reeder R. J., Rector K. D., Donohoe R. J. and Morris D. E. (2004) Spectroscopic investigation of U(VI) sorption at the calcite–water interface. *Geochim. Cosmochim. Acta* **68**(11), 2437–2448.

Fox P. M., Davis J. A. and Zachara J. M. (2006) The effect of calcium on aqueous uranium(VI) speciation and adsorption to ferrihydrite and quartz. *Geochim. Cosmochim. Acta* **70**(6), 1379–1387.

Froideval A., Del Nero M., Barillon R., Hommet J. and Mignot G. (2003) PH dependence of uranyl retention in a quartz/solution system: an XPS study. *J. Coll. Interf. Sci.* **266**(2), 221–235.

Gabriel U., Charlet L., Schlapfer C. W., Vial J. C., Brachmann A. and Gabriel G. (2001) Uranyl surface speciation in silica particles studied by time-resolved laser-induced fluorescence spectroscopy. *J. Colloid Interf. Sci.* **239**(2), 358–368.

Geipel G., Baumann N., Arnold T., Bernhard G., Gerstmann U., Schimmack K. and Read D. (2007) Mobilization and speciation of depleted uranium in water and soils. *Geochim. Cosmochim. Acta* **71**(15), A314.

Giaquinta D. M., Soderholm L., Yuchs S. E. and Wasserman S. R. (1997) The speciation of uranium in a smectite clay: evidence for catalyzed uranyl reduction. *Radiochim. Acta* **76**(3), 113–121.

Glinka Y., Jaroniec M. and Rozenbaum V. M. (1997) Adsorption energy evaluation from luminescence spectra of uranyl ions (UO_2^{2+}) adsorbed on disperse silica surfaces. *J. Colloid Interf. Sci.* **194**, 455–469.

Golub G. H. and Reinsch C. (1970) Singular value decomposition and least squares solutions. *Numer. Math.* **14**(5), 403–420.

Greathouse J. A. and Cygan R. T. (2006) Water structure and aqueous uranyl(VI) adsorption equilibria onto external surfaces of beidellite, montmorillonite, and pyrophyllite: results from molecular simulations. *Environ. Sci. Technol.* **40**(12), 3865–3871.

Grenthe I. and Konings R. J. M. (1992) *Chemical Thermodynamics of Uranium*. North Holland, Elsevier.

Grossmann K., Arnold T., Ikeda-Ohno A., Steudtner R., Geipel G. and Bernhard G. (2009) Fluorescence properties of a uranyl(V)-carbonate species $[U(V)O_2(CO_3)_3]^{5-}$ at low temperature. *Spectrochim. Acta A* **72**(2), 449–453.

Guillaumount R., Fanghänel T., Neck V., Fuger J., Palmer D. A., Grenthe I. and Rand M. H. (2003) *Update on the Chemical Thermodynamics of Uranium, Neptunium, Plutonium, Americium and Technetium*. Amsterdam, Elsevier.

Hennig C., Reich T., Dahn R. and Scheidegger A. M. (2002) Structure of uranium sorption complexes at montmorillonite edge sites. *Radiochim. Acta* **90**(9–11), 653–657.

Hiemstra T., Riemsdijk W. H. V., Rossberg A. and Ulrich K.-U. (2009) A surface structural model for ferrihydrite II: adsorption of uranyl and carbonate. *Geochim. Cosmochim. Acta* **73**(15), 4437–4451.

Hsi C. D. and Langmuir D. (1985) Adsorption of uranyl onto ferric oxyhydroxides: application of the surface complexation site-binding model. *Geochim. Cosmochim. Acta* **49**, 1931–1941.

Hudson E. A., Terminello L. J., Viani B. E., Denecke M. A., Reich T., Allen P. G., Bucher J. J., Shuh D. K. and Edelstein N. M. (1999) The structure of U^{6+} sorption complexes on vermiculite and hydrobiotite. *Clays Clay Miner.* **47**(4), 439–457.

Hunter D. B. and Bertsch P. M. (1998) In situ examination of uranium contaminated soil particles by micro-X-ray absorption and micro-fluorescence spectroscopies. *J. Radio. Nuclear Chem.* **234**, 237–242.

Janney D. E., Cowley J. M. and Buseck P. R. (2000) Transmission electron microscopy of synthetic 2-and 6-line ferrihydrite. *Clays Clay Miner.* **48**(1), 111–119.

Janney D. E., Cowley J. M. and Buseck P. R. (2001) Structure of synthetic 6-line ferrihydrite by electron nanodiffraction. *Am. Mineral.* **86**(3), 327–335.

Jaumot J., Gargallo R., de Juan A. and Tauler R. (2005) A graphical user-friendly interface for MCR-ALS: a new tool for multivariate curve resolution in MATLAB. *Chemometr. Intell. Lab.* **76**(1), 101–110.

Kohler M., Curtis G. P., Kent D. B. and Davis J. A. (1996) Experimental investigation and modeling of uranium(VI) transport under variable chemical conditions. *Water Resour. Res.* **32**(12), 3539–3551.

Kohler M., Curtis G. P., Meece D. E. and Davis J. A. (2004) Methods for estimating adsorbed uranium(VI) and distribution

coefficients of contaminated sediments. *Environ. Sci. Technol.* **38**, 240–247.

Kowal-Fouchard A., Drot R., Simoni E. and Ehrhardt J. J. (2004) Use of spectroscopic techniques for uranium(VI)/montmorillonite interaction modeling. *Environ. Sci. Technol.* **38**, 1399–1407.

Kukkadapu R. K., Zachara J. M., Fredrickson J. K., Smith S. C., Dohnalkova A. C. and Russell C. K. (2003) Transformation of 2-line ferrihydrite to 6-line ferrihydrite under oxic and anoxic conditions. *Am. Mineral.* **88**(11–12), 1903–1914.

Kunze, Q. W. and Dixon, J. B. (1986). Pretreatment for mineralogical analysis. In Klute, A. (ed.), *Methods of Soil Analysis. Part 1. Physical and Mineralogical Methods*. American Society of Agronomy and Soil Science Society of America, Madison, Wisconsin, pp. 91–100.

Liu C. X., Zachara J. M., Zhong L. R., Kukkadupa R., Szecsody J. E. and Kennedy D. W. (2005) Influence of sediment bioreduction and reoxidation on uranium sorption. *Environ. Sci. Technol.* **39**(11), 4125–4133.

Malinowski E. R. (1977) Determination of number of factors and experimental error in a data matrix. *Anal. Chem.* **49**(4), 612–617.

McKinley J. P., Zachara J. M., Smith S. C. and Turner G. D. (1995) The influence of uranyl hydrolysis and multiple site-binding reactions on adsorption of U(VI) to montmorillonite. *Clays Clay Miner.* **43**(5), 586–598.

Michel F. M., Ehm L., Liu G., Han W. Q., Antao S. M., Chupas P. J., Lee P. L., Knorr K., Eulert H., Kim J., Grey C. P., Celestian A. J., Gillow J., Schoonen M. A. A., Strongin D. R. and Parise J. B. (2007) Similarities in 2-and 6-line ferrihydrite based on pair distribution function analysis of X-ray total scattering. *Chem. Mater.* **19**(6), 1489–1496.

Moore D. M. and Reynolds J. R. C. (1997) *X-Ray Diffraction and the Identification and Analysis of Clay Minerals*. New York, Oxford University Press.

Morris D. E., Allen P. G., Berg J. M., Chisholm-Brause C. J., Conradson S. D., Donohoe R. J., Hess N. J., Musgrave J. A. and Tait C. D. (1996) Speciation of uranium in Fernald soils by molecular. *Spectroscopic methods: Characterization of untreated soils. Environ. Sci. Technol.* **30**, 2322–2331.

Morris D. E., Chisholm-Brause C. J., Barr M., Conradson S. D. and Eller P. G. (1994) Optical spectroscopic studies of the sorption of UO_2^{2+} species on a reference smectite. *Geochim CosmaChim. Acta.* **58**, 3613–3623.

Nelson D. O. and Guggenheim S. (1993) Inferred limitations to the oxidation of Fe in chlorite – a high-temperature single-crystal X-ray study. *Am. Mineral.* **78**(11–12), 1197–1207.

Ozaki Y., Ojima S. and Noda I. (2004) 2DCOS-II. *Vibrational Spectrosc.* **36**(2), 141–142.

Pabalan R. T. and Turner D. T. (1997) Uranium (6+) sorption on montmorillonite: experimental and surface complexation modeling study. *Aquat. Geochem.* **2**, 203–226.

Payne T. E., Davis J. A. and Waite T. D. (1996) Uranium adsorption on ferrihydrite – effects of phosphate and humic acid. *Radiochim. Acta* **74**, 239–243.

Phillips T. L., Loveless J. K. and Bailey S. W. (1980) Cr^{3+} Coordination in chlorites – structural study of 10 chromian chlorites. *Am. Mineral.* **65**(1–2), 112–122.

Prikryl J. D., Jain A., Turner D. T. and Pabalan R. T. (2001) Uranium(VI) sorption behavior on silicate mineral mixtures. *J. Contam. Hydrol.* **47**, 241–253.

Qafoku N. P., Zachara J. M., Liu C., Gassman P. L., Qafoku O. and Smith S. C. (2005) Kinetic desorption and sorption of U(VI) during reactive transport in a contaminated Hanford sediment. *Environ. Sci. Technol.* **39**(5), 3157–3165.

Reeder R., Nugent M., Lamble G., Tait C. D. and Morris D. E. (2000) Uranyl incorporation into calcite and aragonite: XAFS and luminescence studies. *Environ. Sci. Technol.* **34**, 638–644.

Reeder R., Nugent M., Tait C. D., Morris D. E., Heald S. M., Beck K. M., Hess W. P. and Lanzirotti A. (2001) Coprecipitation of uranium(VI) with calcite: XAFS, micro-XAS, and luminescence characterization. *Geochim. Cosmochim. Acta* **65**(20), 3491–3503.

Reich T., Moll H., Denecke M. A., Geipel G., Bernhard G. and Nitsche H. (1996) Characterization of hydrous uranyl silicate by EXAFS. *Radiochim. Acta* **74**, 219–223.

Schwertmann U. and Cornell R. M. (2000) *Iron Oxides in the Laboratory Preparation and Characterization*. Wiley-VCH.

Seabaugh J. L., Dong H., Kukkadapu R. K., Eberl D. D., Morton J. P. and Kim J. (2006) Microbial reduction of Fe(III) in the Fithian and Muloorina illites: contrasting extents and rates of bioreduction. *Clays Clay Miner.* **54**, 67–79.

Serne J. R., Brown C. F., Schaef H. T., Pierce E. M., Lindberg M. J., Wang Z., Gassman P. L. and Catalano J. G. (2002) *300 Area Uranium Leach and Adsorption Project*. Richland, WA, Pacific Northwest National Laboratory.

Sherman D. M., Peacock C. L. and Hubbard C. G. (2008) Surface complexation of U(VI) on goethite (α-FeOOH). *Geochim. Cosmochim. Acta* **72**(2), 298–310.

Singer D. M., Maher K. and Brown, Jr., G. E. (2009a) Uranyl-chlorite sorption/desorption: evaluation of different U(VI) sequestration processes. *Geochim. Cosmochim. Acta* **73**(20), 5989–6007.

Singer D. M., Zachara J. M. and Brown, Jr., G. E. (2009b) Uranium speciation as a function of depth in contaminated Hanford sediments – a micro-XRF, micro-XRD, and micro- and bulk-XAFS study. *Environ. Sci. Technol.* **43**(3), 630–636.

Sposito G. and Levesque C. S. (1985) Sodium calcium magnesium exchange on Silver Hill illite. *Soil Sci. Soc. Am. J.* **49**(5), 1153–1159.

Stepanov A. V., Preobrazhenskaya E. B. and Nikitina S. A. (1984) Influence of temperature on the fluorescence of uranyl in frozen solutions of phosphoric and sulfuric acids in the presence of quenchers. *Radiokhmiya* **26**(6), 798–803.

Stubbs J. E., Veblen L. A., Elbert D. C., Zachara J. M., Davis J. A. and Veblen D. R. (2009) Newly recognized hosts for uranium in the Hanford site vadose zone. *Geochim. Cosmochim. Acta* **73**(6), 1563–1576.

Sylwester E. R., Hudson E. A. and Allen P. G. (2000) The structure of uranium (VI) sorption complexes on silica, alumina, and montmorillonite. *Geochim. Cosmochim. Acta* **64**, 2431–2438.

Turner G. D., Zachara J. M., McKinley J. P. and Smith S. C. (1996) Surface-charge properties and UO_2^{2+} adsorption of a subsurface smectite. *Geochim. Cosmochim. Acta* **60**(18), 3399–3414.

Um W., Serne R. J., Brown C. F. and Last G. V. (2007) U(VI) adsorption on aquifer sediments at the Hanford site. *J. Contam. Hydrol.* **93**(1–4), 255–269.

Um W., Serne R. J., Brown C. F. and Rod K. A. (2008) Uranium(VI) sorption on iron oxides in Hanford Site sediment: application of a surface complexation model. *Appl. Geochem.* **23**(9), 2649–2657.

Um W., Zachara J. M., Liu C. X., Moore D. A. and Rod K. A. (2010) Resupply mechanism to a contaminated aquifer: a laboratory study of U(VI) desorption from capillary fringe sediments. *Geochim. Cosmochim. Acta* **74**(18), 5155–5170.

Waite T. D., Davis J. A., Payne T. E., Waychunas G. A. and Xu N. (1994) Uranium (VI) adsorption to ferrihydrite: application of a surface complexation model. *Geochim. Cosmochim. Acta* **58**(24), 5465–5478.

Wan J. M., Kim Y. M., Tokunaga T. K., Wang Z. M., Dixit S., Steefel C. I., Saiz E., Kunz M. and Tamura N. (2009) Spatially resolved U(VI) partitioning and speciation: implications for plume scale behavior of contaminant U in the Hanford vadose zone. *Environ. Sci. Technol.* **43**(7), 2247–2253.

Wang Z., Zachara J. M., Gassman P. L., Liu C., Qafoku O. and Catalano J. G. (2005) Fluorescence spectroscopy of U(VI)-silicate and U(VI)-contaminated Hanford sediment. *Geochim. Cosmochim. Acta* **69**(6), 1391–1403.

Wang Z., Zachara J. M., Liu C., Gassman P. L., Felmy A. R. and Clark S. B. (2008) A cryogenic fluorescence spectroscopic study of uranyl carbonate, phosphate and oxyhydroxide minerals. *Radiochim. Acta* **96**(9–11), 591–598.

Wang Z., Zachara J. M., McKinely J. P. and Smith S. C. (2004a) Cryogenic laser induced U(VI) fluorescence studies of a U(VI) substituted natural calcite: implications to U(VI) speciation in contaminated Hanford sediments. *Environ. Sci. Technol.* **39**, 2651–2659.

Wang Z., Zachara J. M., Yantasee W., Gassman P. L., Liu C. X. and Joly A. G. (2004b) Cryogenic laser induced fluorescence characterization of U(VI) in Hanford vadose zone pore waters. *Environ. Sci. Technol.* **38**(21), 5591–5597.

Zachara J. M., Brown C., Christensen J., Dresel E., Kelly S., Liu C., McKinley J. and Um W. (2007) *A Site-Wide Perspective on Uranium Geochemistry at the Hanford Site*. Pacific Northwest National Laboratory Richland, WA.

Zachara J. M., Davis J. A., Liu C., McKinley J. P., Qafoku N., Wellman D. M. and Yabusaki S. (2005) *Uranium Geochemistry in Vadose Zone and Aquifer Sediments from the 300 Area Uranium Plume, PNNL-15121*. Pacific Northwest National Laboratory Richland, WA.

Zachara J. M. and McKinley J. P. (1993a) Influence of hydrolysis on the sorption of metal cations by smectite: importance of edge coordination reactions. *Aquat. Sci.* **55**(4), 250–261.

Zachara J. M., Smith S. C., McKinley J. P. and Resch C. T. (1993b) Cadmium sorption on specimen and soil smectites in sodium and calcium electrolytes. *Soil Sci. Soc. Am. J.* **57**(6), 1491–1501.

Associate editor: Peggy A. O'Day